AC conductivity of amorphous and polycrystalline Cd_3As_2 films on single crystal substrates of Al_2O_3

A.A. Morocho [*], E.A. Pilyuk, V.S. Zakhvalinskii, T.B. Nikulicheva, M.N. Yapryntsev, V.Yu. Novikov

Belgorod National Research University, Belgorod, 308015, Russia

ARTICLE INFO

ABSTRACT

In this work, we present first AC conductivity measurements of both amorphous and polycrystalline Cd_3As_2 thin films ($\sim$ 50 nm) in the frequency range 25–10^6 Hz and temperature range 10–300 K. Cd_3As_2 thin films were grown by non-reactive AC magnetron sputtering. Both samples show a strong frequency dependence of the total conductivity in the order of 10^4 Ω^{-1} cm^{-1}. It was found that the DC conductivity, deduced from the total conductivity of Cd_3As_2 thin films, increases with increasing temperature. The experimental results indicate exponent values s> 1 and s>2, which contradicts the universal dynamic response. In Cd_3As_2 films is observed a crossover of metal–semiconductor type at low temperatures, which is characteristic of topological materials. The results show a clearly frequency dependence of the mechanism of AC conductivity of Cd_3As_2 films in a wide range of temperatures.

1. Introduction

During the last decades, the well know topological Cd_3As_2 and Cd_3As_2-based compounds became one of the most intensively studied materials of condensed matter physics, and have presented a large field of research both experimentally and theoretically. Indeed, this great interest in this type of materials was due to their potential applications in electronics, spintronics and functional devices. Cd_3As_2 is identified as an ideal Dirac semimetal showing chemical stability in air [1], with a declared mobility well above 10^6 $cm^2/(V\ s)$ [2]. To understand the electronic properties of Cd_3As_2, and extraordinarily large mobility of electrons in particular, theoretical models have been proposed in the standard framework of DC theory. However, there are not reports available on AC conductivity properties of Cd_3As_2 and narrow-gap semiconductors. As both the DC and AC conductivity can be due to different independent processes, analysis of AC conductivity of Cd_3As_2 provides important information related to charge transfer by carriers, which dominate the conduction process, and their response to changes in temperature and frequency. A convenient formalism to investigate the frequency dependence of conductivity in a variety of materials is based on the power law relation proposed by Jonscher and is used to describe the electrical conductivity of many types of disordered solids [3]. In order to correlate the nature of frequency exponent values as a function of temperature $s(T)$ with a proposed conduction

mechanism, several theoretical models have been developed [3] with frequency exponent values s in the range $0 < s < 1$. However, the literature endorsed that the exponent values s is not limited to values below 1 [4] and experimentally obtained values for $s > 1$ have been reported in a lot of cases concerning dielectric measurements for different types of disordered materials at a frequency range below 1 MHz [5].

It is well known that the AC conductivity study of glassy systems in a wide range of temperatures and frequencies is essential for material researchers not only for practical applications but also for academic interest especially due to their amorphous semiconducting nature and technological applications in wide fields [6–11]. However, the topological Cd_3As_2 bellows to another class of materials. Recent experimental data for the topological Cd_3As_2 demonstrate Shubnikov–de Haas oscillations, colossal linear magnetoresistance, photovoltage generation across a metal/Cd_3As_2 nano crystal contact, and an unconventional photoelectromagnetic effect [12]. Although at first Cd_3As_2 amorphous films were considered as new amorphous semiconductor materials with unusual properties especially at low temperatures and high magnetic fields, where clear Shubnikov–de Haas oscillations have been observed, there were some fundamental differences [13] that make these amorphous materials a special class of materials and therefore cannot be treated as usual amorphous solids. A clear example is that the values of the Hall mobility for these films are one to four
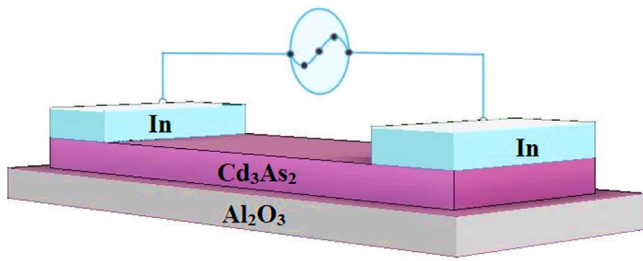
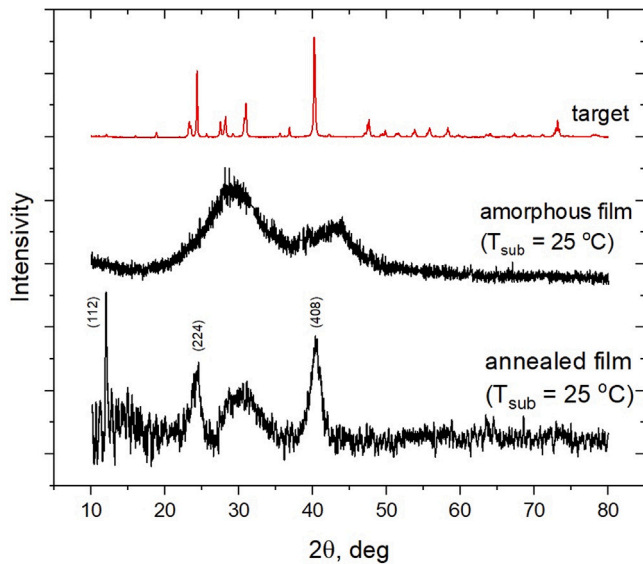**Fig. 1.** Schematic diagram of AC measurements of Cd₃As₂ films.

Fig. 2. X-ray diffraction patterns of Cd₃As₂ films and target.

orders in magnitude higher than those of other amorphous materials [13]. In addition to both transport and optical properties polycrystalline Cd₃As₂ films reported in [13–15], experimental observations of superconductivity were reported [16,17] for polycrystalline Cd₃As₂ thin films without application of any external factors, which makes polycrystalline Cd₃As₂ thin films a promising platform for studies of topological superconductivity state and other related phenomena.

The main objective of the present work is to study the AC conductivity response of the topological semimetal Cd₃As₂ in a wide range of temperatures. AC conductivity measurements have been carried out in two different Cd₃As₂ systems (amorphous and polycrystalline thin films) to acquire a better understanding of the structure contribution to AC conductivity response at various temperatures. Although the modern theory of AC conductivity can explain many transport phenomena of materials such as amorphous semiconductors, disordered and ionic solids, the AC mechanisms which are present in both narrow-gap semiconductors and topological materials are not clear at the present time due to the complexity of AC conductivity phenomena that can exist in these materials at different temperatures.

2. Experimental

Cd₃As₂ thin films were grown by non-reactive AC magnetron sputtering in argon atmosphere on oriented (0001) α–Al₂O₃ single crystal substrates. Since (0001) α–Al₂O₃ and (224) α–Cd₃As₂ have a similar structure and their average interatomic (interstitial) distances differ by only 6%, well-oriented film growth can be achieved [12]. Substrate heating was not carried out, the substrate temperature T_{sub} was equal to room temperature and did not change during deposition. Thus,
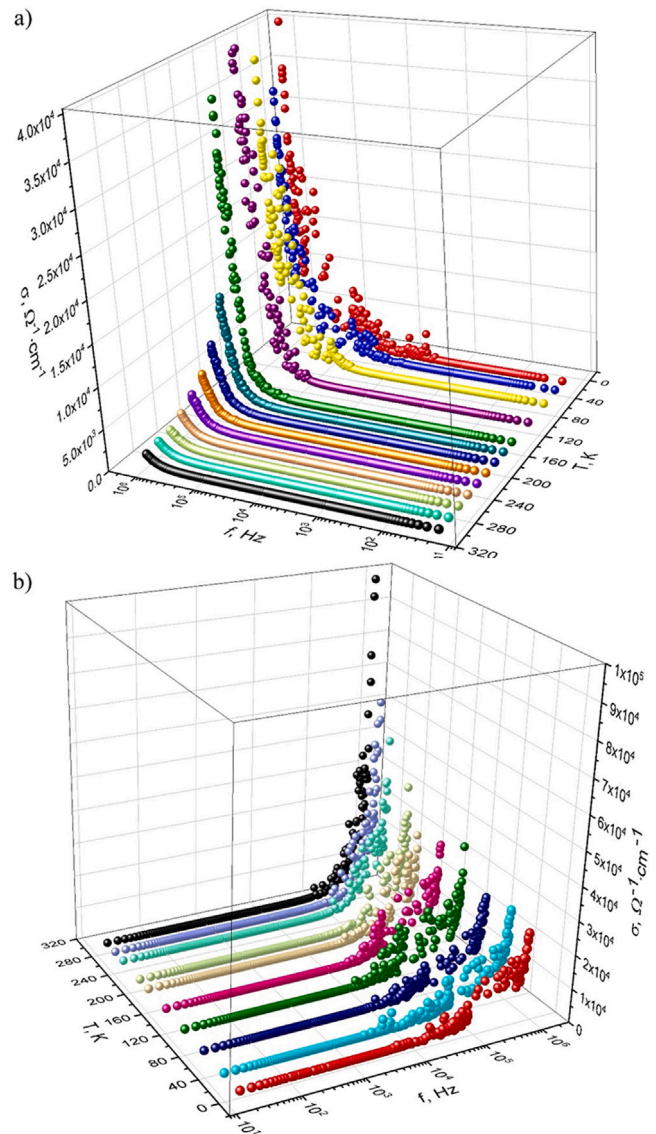

Fig. 3. Frequency dependences of the total conductivity σ at different temperatures: (a) for the amorphous Cd₃As₂ film; (b) for the polycrystalline Cd₃As₂ film.

two types of films were obtained: (1) amorphous thin films without heating the substrates at room temperature and (2) polycrystalline thin films in Ar atmosphere at a temperature of 573 K for 5 min after deposition without heating the substrates. The thickness of the films was determined by deposition time and was 50 nm. Films with a thickness of 50 nm can be considered as a two-dimensional system, and the manifestation of quantum effects is possible [18]. Furthermore, the resistivity increases with decreasing film thickness [19]. The phase composition of the grown films was almost stoichiometric, which was confirmed by Energy-Dispersive X-ray Analysis (Nova NanoSem 450, FEI Company), which demonstrates that the actual elemental composition is close to the stoichiometric Cd₃As₂, with ratio Cd/As = 1.59. The crystal structure of the films under study was determined using a Rigaku SmartLab X-ray diffractometer (CuKα radiation, $\lambda = 1.5401$ Å) at room temperature. Frequency dependencies of the conductivity of Cd₃As₂ thin films were measured using an AKTAKOM AM-3026 high frequency RLC meter in the medium frequency range from 25 Hz to 1 MHz and temperatures from 10 to 300 K using a setup based on a Janis CCS-350S closed cycle helium cryostat and a temperature regulator model Lakeshore 331. Shielded 4-wire Kelvin probes were used in the
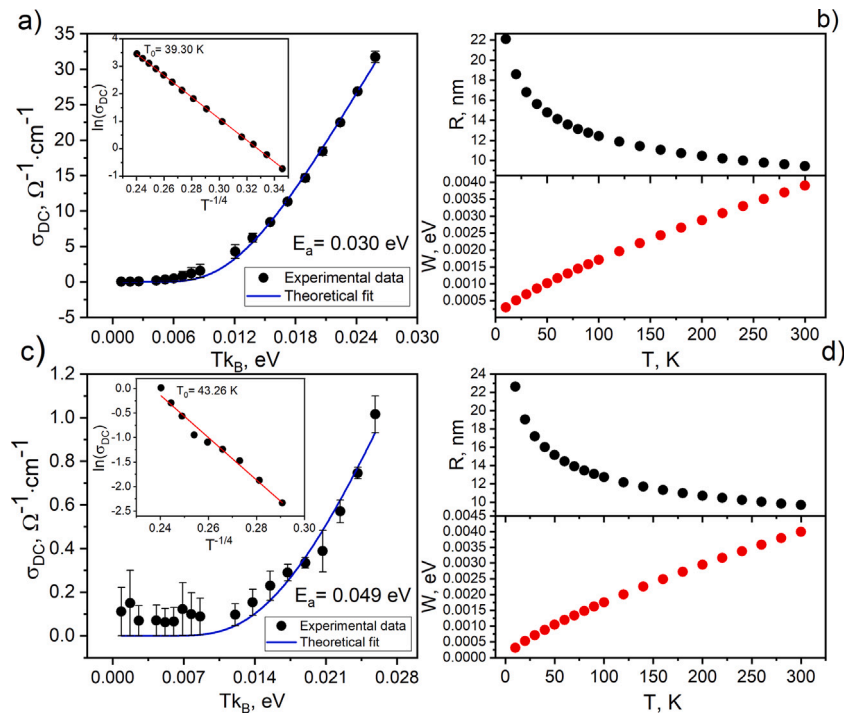
Fig. 4. Temperature dependences of DC conductivity, average hopping distance (R) and average hopping energy (W): (a, b) for the amorphous Cd_3As_2 film; (c, d) for the polycrystalline Cd_3As_2 film. Insets describe the linear $\ln \sigma_{DC}$ vs $T^{-1/4}$ plots.

measurements, which were connected directly to the output connector of the helium cryostat. The wires from the sample to the connector inside the chamber were twisted. The noise did not exceed 1%. The data were recorded using a PC system under isothermal conditions, and the temperature was stabilized with an accuracy better than 0.005 K. The measurements were carried out by a two-contact method in coplanar geometry (Fig. 1). Indium contacts were deposited on the sample surface by magnetron sputtering in a VN-2000 vacuum system.

3. Results and discussion

Fig. 2 shows X-ray diffraction patterns of Cd_3As_2 films on Al_2O_3 single crystal substrates. X-ray diffraction patterns of Cd_3As_2 films deposited on cold substrates show broad peaks (amorphous halo peaks) usually attributed to amorphous materials. Annealing of the films leads to partial crystallization with three pronounced peaks at $2\theta \approx 12°$, 24.5° and 40.3°, corresponding to the α modification of Cd_3As_2 with a tetragonal lattice (space group $I4_1/acd$) [20]. The fact that the ratios between intensities of the observed peaks are close to relative intensities of the target material (1 mm Cd_3As_2 single crystals placed in a round copper cell with diameter 40 mm and deep 4 mm) indicates the absence of any pronounced orientation of Cd_3As_2 crystallites in the films under study. Using the standard Debye–Scherrer equation:

$$L = \frac{0.9\lambda}{\beta cos(\theta)} \tag{1}$$

where $\lambda = 1.5401$ Å, β is the peak width at half height, θ is the diffraction angle, we estimated the mean crystallite size to be 6–8 nm. It is well know that the AC conductivity analysis provides significant information related to transport of charge carriers, i.e., electron/holes or cations/anions that predominate the conduction process and their response as a function of temperature and frequency [21]. Thus, the transport phenomena and charge carrier dynamics within the material can be well understood by the analysis of the frequency dependence of AC conductivity [22]. Frequency dependencies of the total conductivity σ at different temperatures are shown in Fig. 3 for both amorphous and

polycrystalline Cd_3As_2 films. The total conductivity σ [21] over a wide range of frequencies f and temperatures T can be written as:

$$\sigma = \sigma_{AC} + \sigma_{DC} \tag{2}$$

where σ_{AC} is the AC conductivity and σ_{DC} is the DC conductivity. In general, frequency dependencies of σ usually show two distinct regions: (1) the low-frequency region (almost frequency independent conductivity) and (2) the high-frequency region (dispersion region). The presence of these regions and the increase of total conductivity with increasing frequency is characteristic for disordered solids, oxides, and nanocomposites [3]. The dispersion region, corresponding, in most cases, to the high frequency region of the total conductivity, obeys the Jonscher's power law $\sigma_{AC} = A\omega^s$, where A is a constant depending on temperature, ω is the angular frequency ($\omega = 2\pi f$ where f is the frequency) and s is the frequency exponent which is frequently applied to comprehend the mechanism of electrical conduction in disordered matter [3] such as amorphous semiconductors, disorder and ionic glasses [8]. Both A and σ_{DC} are regarded as thermally activated quantities [23]. The quantity $\sigma_{AC}(\omega)$ is frequency dependent conductivity which is used to analyze and understand the dynamics of the charges [22].

In Fig. 3, the curves show a strong frequency dependence of total conductivity in the order of 10^4 $\Omega^{-1}cm^{-1}$. For both samples, the total conductivity decreases with decreasing frequency and becomes almost independent at frequencies below $\sim 10^4$ Hz. Thus, regions where total conductivity is almost constant, reveal a main contribution of DC conductivity, while AC conductivity contribution begins to be the dominant in different frequency regions for each temperature. On the other hand, the amorphous Cd_3As_2 film is also characterized by a decrease in total conductivity values with increasing temperature while the polycrystalline Cd_3As_2 film shows higher values of total conductivity at high temperatures. According to [24], at lower frequencies, grain boundaries are effective with high resistance giving a constant conductivity, whereas at higher frequencies, the increase in conductivity is due to grains with much higher conductivity and also due to increase in hopping of charge carriers, which is accompanied by the increase of temperature. Moreover, the frequency dependence of
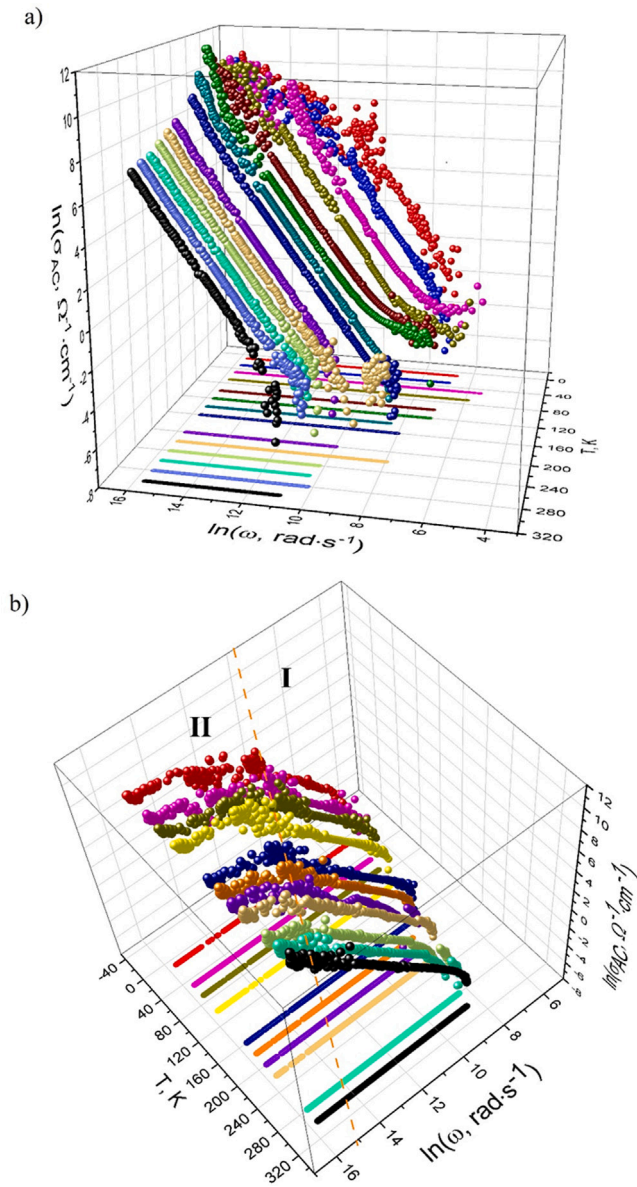
a)

b)

Fig. 5. $\ln \sigma_{(AC)}$ vs $\ln(\omega)$ at different temperatures of (a) amorphous and (b) polycrystalline Cd_3As_2 films.

conductivity does not follow the simple power relation as given above but follows a double power law, which is demonstrated later:

$$\sigma = \sigma_{DC} + A\omega^{s1} + A\omega^{s2} \tag{3}$$

In Fig. 4, the temperature dependence of DC conductivity is presented for both amorphous and polycrystalline samples. According to the universal expression (2), the DC conductivity is estimated from total conductivity vs. frequency measurements. Therefore, the DC conductivity part should be less informative than the real part of the AC conductivity [25]. As one can see, the DC conductivity increases with increasing temperature, confirming a thermally activated transport process in the conduction mechanism. Since the conduction mechanism satisfies the Arrhenius law, the activation energy can be given by equation as follows:

$$\ln \sigma_{DC} = \ln \sigma_0 - \frac{E_a}{k_B} \frac{1}{T} \tag{4}$$

where σ_0 is the pre-exponential term, E_a is the activation energy for conduction, k_B is the Boltzmann constant and T is the measurement

temperature. It can be seen that the fit (blue solid line in Fig. 4) matches well with the experimental values of the amorphous Cd_3As_2 film, while in the case of polycrystalline film we observe that the theoretical fit of σ_{DC} does not match up well with experimental values at low temperatures. This discrepancy between theoretical fit and experimental values at low temperatures may be due to a change of conduction mechanism in the polycrystalline film. The values of activation energy E_a deduced from the linear fit are E_a = 0.030 and 0.049 eV for the amorphous and polycrystalline samples, respectively.

From the slope $\ln \sigma_{DC}$ vs $T^{-1/4}$ (Fig. 4, insets), we can determine the value of the parameter T_0 — a constant proportional to the density of states near the Fermi level $N(E_F)$ which is nearly equal to $T_0 \approx 39$ and 43 K for the amorphous and polycrystalline sample, respectively. The density of localized states near the Fermi level was calculated by the formula [26]:

$$N(E_F) = \frac{\lambda}{T_0 k_B r^3} \tag{5}$$

where λ is a dimensionless constant equal to 18–49 [26]. The main values of $N(E_F)$ of the amorphous and polycrystalline film obtained from (5) are $0.727 \cdot 10^{20}$ and $0.66 \cdot 10^{20} eV \cdot cm^3$, respectively. Ambegaokar et al. showed that the lower limit of the value of λ is about 16 [27]. The carrier localization radius was taken equal to r = 41.8 nm [28]. The average hopping distance R and the average hopping energy W were estimated using the following equations [29,30].

$$R = \left(\frac{9}{8\pi K_B T N(E_F)}\right)^{1/4} \tag{6}$$

$$W = \left[\frac{3}{4\pi R^3 N(E_F)}\right] \tag{7}$$

As shown for both samples in Fig. 4(b) and (d), with decreasing temperature, the hopping distance increase and hopping activation energy decreases. Thus, there will be an optimum hopping distance (R), which maximizes the hopping probability [31]. A hopping electron will always try to find the lowest activation energy and the shortest hopping distance. However, usually the two conditions cannot be satisfied at the same time [31]. From the slope $\ln(\sigma_{AC})$ vs $\ln(\omega)$ in Fig. 5, it is possible to determine the values of frequency exponent s (see Fig. 6), which for the amorphous sample are in the range (1<s<2.2) and increases slightly with increasing temperature. For the polycrystalline sample, dependences of $\ln(\sigma_{AC})$ vs $\ln(\omega)$ show the presence of two different regions I and II that correspond to the regimens ($1.6<s_1<2.3$) and ($0.2<s_2<1.2$), respectively. Different models such as the quantum mechanical tunneling (QMT), the correlated barrier hopping (CBH), the overlapping large-polaron tunneling (OLPT), and the non-overlapping small polaron tunneling (NSPT), have been considered to account for the AC conduction mechanism [32]. All the above-mentioned models show s values only in the range 0<s<1, i.e., the classical AC theory with 0<s<1 is not applicable to our samples. On the other hand, it was confirmed in [4] that the exponent s is not limited to values below 1. In general, the frequency dependence of the conductivity does not obey a simple power law. As far as we know, there are not rigorous published studies that can explain the universal meaning for s> 1 in materials which are not disordered or ionic solids. However, there are studies [33–35] which give an explanation of s values 1<s<2, based on the jump relaxation model (JRM) introduced by Funke (1993) for ionic conduction in solids [36]. As is mentioned in [36], values in the range 1<s<2 are a significant aspect of low temperature/high frequency process. On the other hand, it was demonstrated in [37] that in the limit of low frequencies, the exponent of the frequency-dependent term must be 2 instead of s<1, and at high frequencies, the Jonscher's power law cannot hold either, since an unlimited increase of the conductivity is unphysical. The Jonscher's universal law, where s is a fractional exponent roughly treated as constant less than 1, is often used to describe the AC component contributing to the dispersive region. Although such behavior is observed in entirely different types
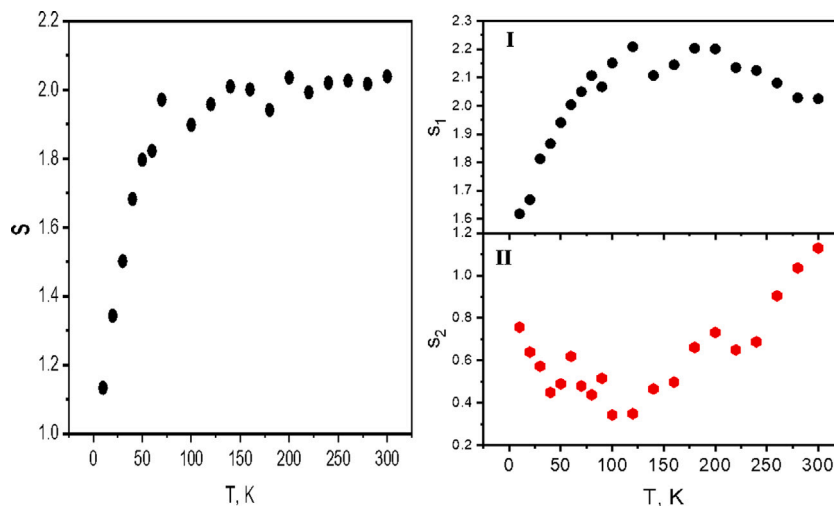
Fig. 6. Temperature dependence of the frequency exponent s of (right) amorphous and (left) polycrystalline Cd_3As_2 films.
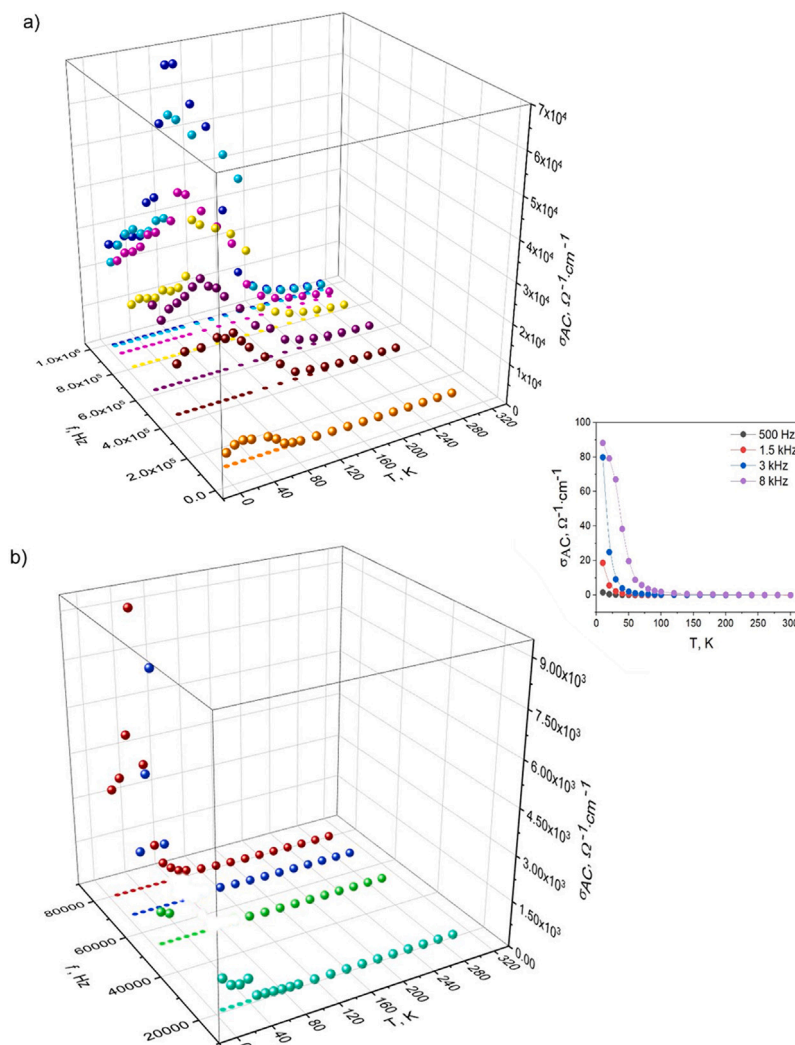

Fig. 7. Temperature dependence of σ_{AC} of the amorphous Cd_3As_2 film in the frequency range (a) $10^5 - 10^6$ Hz and (b) $2 \cdot 10^4 - 8 \cdot 10^5$ Hz. The inset shows temperature dependence of σ_{AC} at frequencies < 8 kHz.

of materials, such as disordered semiconductors, polymers, conducting polymer compound ceramics, ion conducting glasses, heavily doped ionic crystals, etc. [4], experimentally obtained values of s> 1 have been also reported for different types of disordered materials at a frequency range below 1MHz [5]. Although, several models on the hopping or tunneling of polarons between equilibrium sites have been
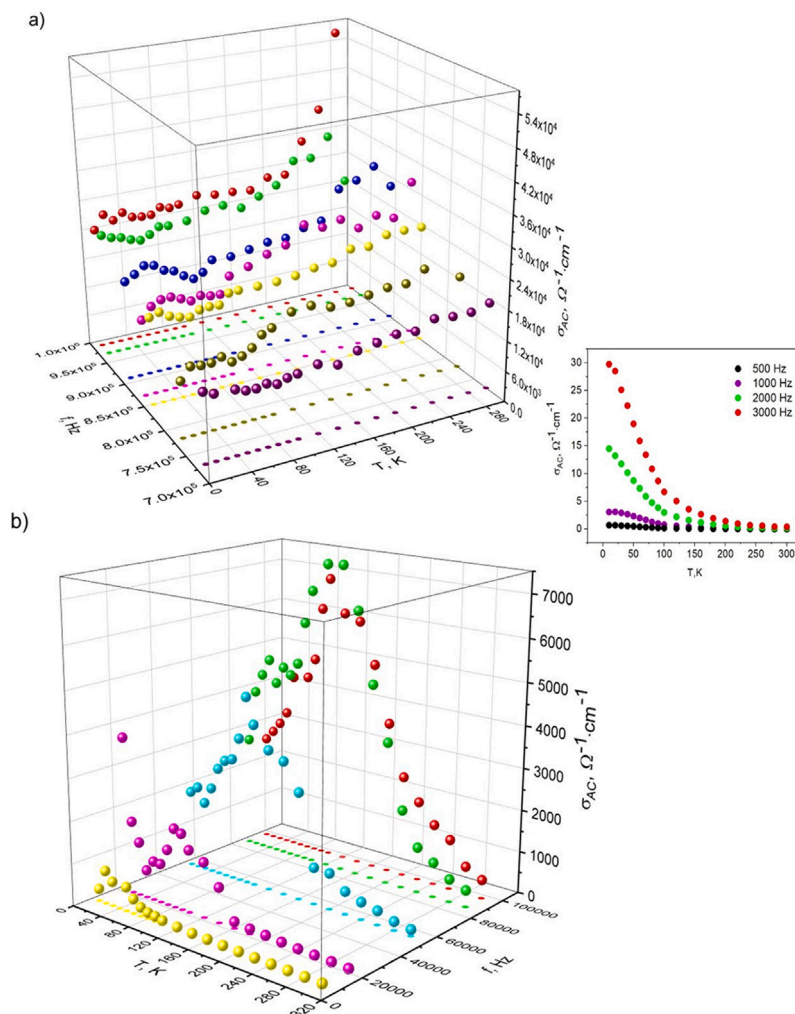
a)

b)

Fig. 8. Temperature dependence of σ_{AC} of the polycrystalline Cd_3As_2 film in the frequency range (a) $7 \cdot 10^5 - 10^6$ Hz and (b) $10^4 - 10^5$ Hz. The inset shows temperature dependence of σ_{AC} at frequencies < 3 kHz.

established to explain the frequency and temperature dependence of the AC conductivity within different limited temperature ranges, but it still needs more insight [38]. At the present time, the universal frequency dependence of electric and dielectric properties of disordered ionic materials is described by different authors in different ways. The power-law treatment is still very popular, but it has also been realized that the power-law frequency dependence is not necessarily a law of nature [37].

Both Figs. 7 and 8 show temperature dependencies of AC conductivity in a medium frequency range for both types of samples. It can be immediately seen that the temperature behavior of AC conductivity changes over a wide frequency range. However, at low frequencies the curves show a similar behavior, although in the case of the amorphous film the AC conductivity values are much higher than the polycrystalline one. Figs. 7 and 8 indicate a change in the AC conduction mechanism. For deeper analysis, we plotted temperature dependences of AC resistivity, $\rho_{AC} = 1/\sigma_{AC}$, at different frequencies for both samples (Figs. 9 and 10). For the amorphous sample, below the temperature T*, ρ_{AC} changes from its linear T-behavior at high temperatures and exhibits a pronounced minimum T_{min} at low temperatures. A deviation of $\rho_{AC}(T)$ indicates a metal–semiconductor crossover; ρ_{AC} saturates at low temperature.

This indicates that the ground state is metallic, and therefore T* marks the beginning of the transition from the metallic state to another state. T* is identified as the onset of the pseudogap phase, following the standard definition: the temperature below which the AC conductivity

(or AC resistivity) begins to deviate from its linear T-behavior at high temperatures [39,40]. The deviation of ρ can be either upward, as in LSCO, or downward, as in $YBa_2Cu_3O_y$ [39], depending on the relative magnitude of inelastic and elastic (disorder) scattering at T*; in $YBa_2Cu_3O_y$, the copper oxide material with the least random scattering, the loss of inelastic scattering below T* is a much larger relative effect than in LSCO, hence the drop in ρ [39]. As one can see, a significant change in ρ_{AC} emerges around T_{min}, where the AC resistivity shows a transition to semiconductor behavior in a wide range of frequencies. This transition behavior becomes notable even at lower frequencies, and the transition temperature also changes depending on the frequency. After crossover, the resistivity soon becomes saturated, forming a stable resistivity plateau in the low temperature region. A similar low-temperature resistivity plateau is observed in topological semimetals and does not depend on the quality of the sample [41–45]. Therefore, such a low-temperature resistivity saturation is an intrinsic property of topological semimetals [46], Although, the metal–semiconductor transition, induced by a magnetic field, is often described as the result of opening a gap at the points of contact between bands in topological semimetals [41–45], in our case, the reason for this behavior has not yet been settled.

On the other hand, for the polycrystalline sample, Fig. 10 shows a metal–semiconductor transition at temperatures below $\sim$ 100 K (transition observed in the amorphous Cd_3As_2 film), which is an intrinsic property of topological semimetals [46]. However, with decreasing frequency, an increase in AC resistivity is also observed at temperatures
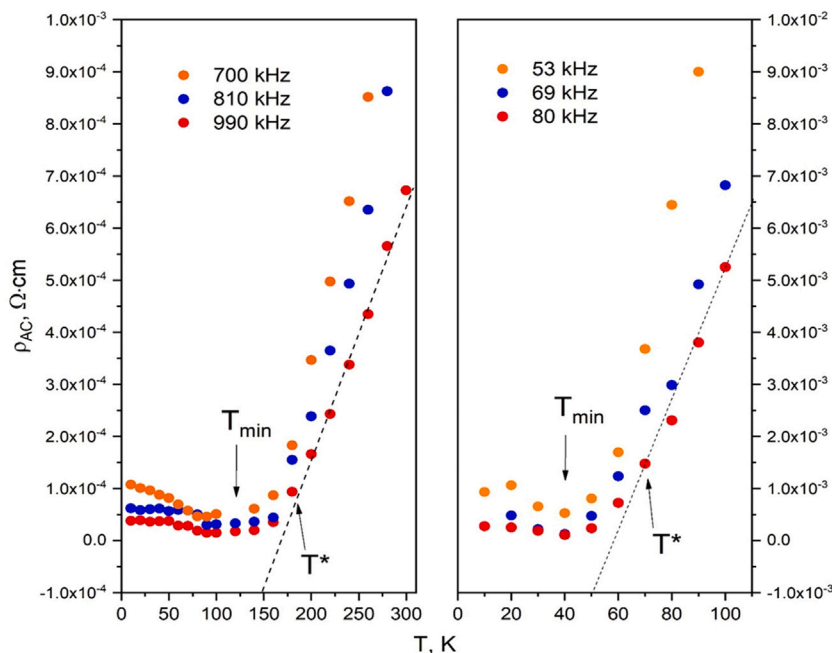
Fig. 9. Temperature dependence of AC resistivity $\rho_{AC}(T)$ of the amorphous Cd$_3$As$_2$ film at different frequencies. The dashed lines illustrate the linear T-behavior of AC resistivity.
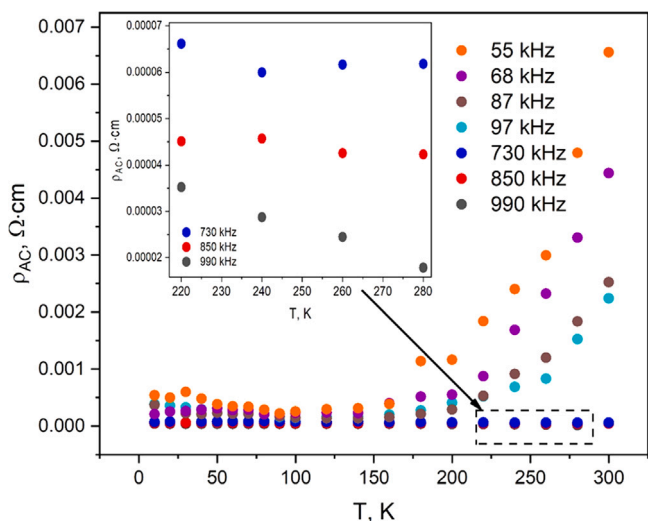

Fig. 10. Temperature dependence of the AC resistivity of the polycrystalline Cd$_3$As$_2$ film at different frequencies.

> 150 K and below the critical frequency of ∼ 730 kHz, the behavior of $\rho_{AC}(T)$ changes significantly at higher temperatures; $\rho_{AC}(T)$ curve begins to deviate upward showing a transition of metal–semiconductor type. In presence of magnetic field, this behavior of resistivity is only observed at low temperatures in several topological semimetals [41,42, 47].

One reasonable explanation for the increase of ρ_{AC} is scattering at grain boundaries formed during annealing. At frequencies < 730 kHz, ρ_{AC} of the polycrystalline Cd$_3$As$_2$ film begins to increase, which indicates strong scattering at grain boundaries and, therefore, a lower carrier mobility in the polycrystalline Cd$_3$As$_2$ film at temperatures > 150 K. In Fig. 11 (left) we plotted $\ln(\rho_{AC})$ as a function of T^{-1}, which can be used to estimate the energy gap Eg according to the relation $\rho_{AC} \propto exp(E_g/2k_BT)$ as in the case of narrow-gap semiconductors and topological materials [42,46,48]. The resulting gap values are plotted as a function of frequency in Fig. 11 (right). As the curves are

linear over a very small temperature range, the calculated energy gap depends on the region of linear fitting and hence becomes a function of T. Furthermore, the calculated energy gap clearly exhibits a strong frequency dependence for the polycrystalline film of Cd$_3$As$_2$, which has never been observed before.

It is well know that Cd$_3$As$_2$ is among the most explored materials in solid-state physics [2] and has been well-studied in the past [49]. Among a number of Dirac semimetal materials, Cd$_3$As$_2$ has its own advantages and unique properties [50] and possesses many of the same interesting optoelectronic properties as graphene with the additional benefit of possessing a strong light–matter interaction conferred by its 3D nature [51]. However, at the present time, there are not current studies with AC measurements in this material. Thus, the present work not only shows an important experimental contribution in the area of AC conductivity measurements but also represent a step toward the manipulation of the topological semimetal Cd$_3$As$_2$ via changing the AC frequency.

4. Conclusion

The analysis of the frequency dependence of the total AC conductivity of both amorphous and polycrystalline films showed different temperature response. In both samples, the DC conductivity increased with the increase of temperature. Both amorphous and polycrystalline samples showed exponent values of s>1. However, in the polycrystalline film was a observed the presence of two regions denoted as I and II in curves $ln(\sigma_{AC})$ vs $ln(\omega)$ with exponent values s> 1 and s>2, respectively. These results completely contradict the universal dynamic response for all the models suggested for the AC theory. In both Cd$_3$As$_2$ films, a metal–semiconductor crossover was found at low temperatures, which is an intrinsic characteristic of topological semimetals. A change in the behavior of the conduction mechanism in the high temperature region was found in the polycrystalline Cd$_3$As$_2$ film, suggesting strong scattering at grain boundaries and, therefore, a lower carrier mobility film at high temperatures. Furthermore, the calculated energy gap clearly showed a strong frequency dependence for the polycrystalline Cd$_3$As$_2$ film. Our results not only provide a new research direction of topological semimetals, but also bring insights to AC conductivity measurements of non-disordered materials.
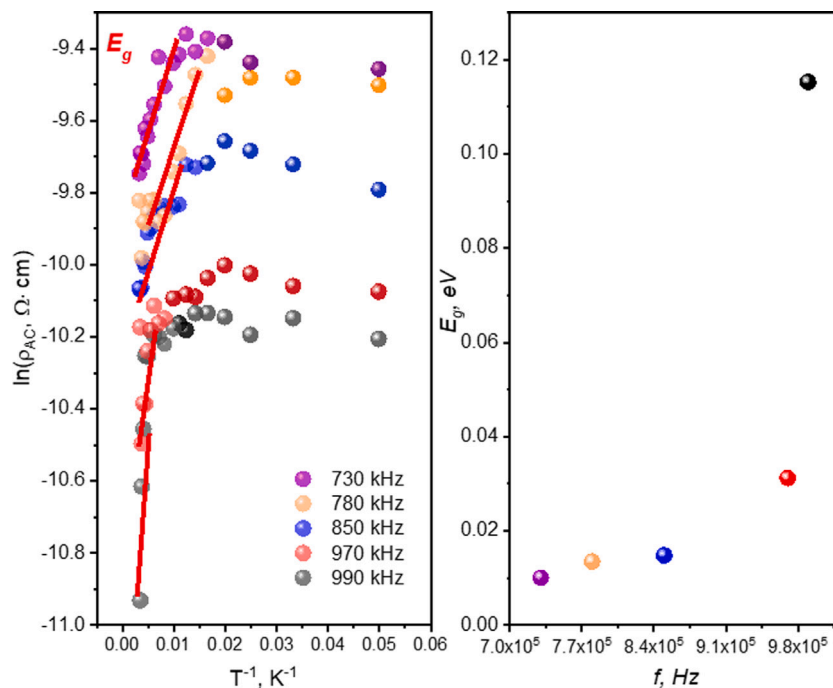
Fig. 11. $\ln(\rho_{AC})$ as a function of T^{-1} (left) and frequency dependence of the energy gap (right) for the polycrystalline film. Red solid lines indicates the regions of the linear fit.

CRediT authorship contribution statement

A.A. Morocho: Supervision, Writing – review & editing. **E.A. Pilyuk:** Project administration, Conceptualization. **V.S. Zakhvalinskii:** Resources. **T.B. Nikulicheva:** Formal analysis. **M.N. Yapryntsev:** Investigation. **V.Yu. Novikov:** Investigation.

Declaration of competing interest

The authors declare that they have no known competing financial interests or personal relationships that could have appeared to influence the work reported in this paper.

References

[1] S. Nishihaya, M. Uchida, Y. Nakazawa, M. Kriener, Y. Kozuka, Y. Taguchi, M. Kawasaki, Gate-tuned quantum hall states in Dirac semimetal $(Cd_{1-x}Zn_x)_3As_2$, Sci. Adv. 4 (5) (2018) eaar5668, http://dx.doi.org/10.1126/sciadv.aar5668.

[2] I. Crassee, R. Sankar, W.-L. Lee, A. Akrap, M. Orlita, 3D Dirac semimetal Cd_3As_2: A review of material properties, Phys. Rev. Mater. 2 (2018) http://dx.doi.org/10.1103/PhysRevMaterials.2.120302.

[3] A. Radoń, D. Łukowiec, M. Kremzer, J. Mikuła, P. Włodarczyk, Electrical conduction mechanism and dielectric properties of spherical shaped Fe_3O_4 nanoparticles synthesized by co-precipitation method, Materials 11 (5) (2018) http://dx.doi.org/10.3390/ma11050735.

[4] A. Papathanassiou, I. Sakellis, J. Grammatikakis, Universal frequency-dependent ac conductivity of conducting polymer networks, Appl. Phys. Lett. 91 (2008) http://dx.doi.org/10.1063/1.2779255.

[5] C. Tsonos, Comments on frequency dependent AC conductivity in polymeric materials at low frequency regime, Curr. Appl. Phys. 19 (4) (2019) 491–497, http://dx.doi.org/10.1016/j.cap.2019.02.001.

[6] A. Chamuah, K. Bhattacharya, M. Sahidul Ali, D. Ghosh, D. Chattopadhyay, S. Bhattacharya, Density of states, DC conductivity and physical properties of Ag_2S–Ge–Te–Se chalcogenide glassy system, Appl. Phys. A 127 (2021) 656, http://dx.doi.org/10.1007/s00339-021-04796-z.

[7] A. Acharya, K. Bhattacharya, C. Kumar Ghosh, A. Narayan Biswas, S. Bhattacharya, Charge carrier transport and electrochemical stability of Li_2O doped glassy ceramics, Mater. Sci. Eng. B 260 (2020) 114612, http://dx.doi.org/10.1016/j.mseb.2020.114612.

[8] S. Bhattacharya, AC conductivity behaviour and charge carrier concentrations of some vanadate glassy system, Phys. Lett. A 384 (16) (2020) 126324, http://dx.doi.org/10.1016/j.physleta.2020.126324.

[9] S. Bhattacharya, R. Kundu, K. Bhattacharya, A. Poddar, D. Roy, Micromechanical hardness study and the effect of reverse indentation size on heat-treated silver doped zinc-molybdate glass nanocomposites, J. Alloys Compd. 770 (2019) 136–142, http://dx.doi.org/10.1016/j.jallcom.2018.08.085.

[10] S. Bhattacharya, A. Ghosh, Conductivity relaxation in iodomolybdate glass-nanocomposites embedded with ZnO nanoparticles and α-AgI nanocrystals, J. Nanosci. Nanotechnol. 7 (2007) 3684–3688, http://dx.doi.org/10.1166/jnn.2007.808.

[11] S. Mandal, A. Ghosh, Structure and physical properties of glassy lead vanadates, Phys. Rev. B 48 (1993) 9388–9393, http://dx.doi.org/10.1103/PhysRevB.48.9388.

[12] A. Kochura, V. Zakhvalinskiǐ, Z.H.A. Zaw Htet Aung, A. Ril, E. Pilyuk, A. Kuz'menko, B. Aronzon, S. Marenkin, Growth of thin cadmium arsenide films by magnetron sputtering and their structure, Inorg. Mater. 55 (2019) 879–886, http://dx.doi.org/10.1134/S002016851909005X.

[13] C. Weclewicz, L. Żdanowicz, Transport properties of thin amorphous films of cadmium arsenide, Thin Solid Films 151 (1) (1987) 87–101, http://dx.doi.org/10.1016/0040-6090(87)90011-3.

[14] A. El-Shazly, H. Soliman, D.A. El-Hady, H. El-Sayed, Optical properties of Cd_3As_2 polycrystalline thin films, Vacuum 47 (1) (1996) 53–56, http://dx.doi.org/10.1016/0042-207x(95)00195-6.

[15] N. Kovaleva, L. Fekete, D. Chvostova, A. Muratov, Morphology and optical properties of thin Cd_3As_2 films of a Dirac semimetal compound, Metals 10 (10) (2020) http://dx.doi.org/10.3390/met10101398.

[16] A.V. Suslov, A.B. Davydov, L.N. Oveshnikov, L.A. Morgun, K.I. Kugel, V.S. Zakhvalinskii, E.A. Pilyuk, A.V. Kochura, A.P. Kuzmenko, V.M. Pudalov, B.A. Aronzon, Observation of subkelvin superconductivity in Cd_3As_2 thin films, Phys. Rev. B 99 (2019) 094512, http://dx.doi.org/10.1103/physrevb.99.094512.

[17] L. Oveshnikov, A. Davydov, A. Suslov, A. Ril, S. Marenkin, A. Vasiliev, B. Aronzon, Superconductivity and Shubnikov - de Haas effect in polycrystalline Cd_3As_2 thin films, Sci. Rep. 10 (2020) 4601, http://dx.doi.org/10.1038/s41598-020-61376-6.

[18] B. Zhao, P. Cheng, H. Pan, S. Zhang, B. Wang, G. Wang, F. Xiu, F. Song, Weak antilocalization in Cd_3As_2 thin films, Sci. Rep. 6 (2016) 22377, http://dx.doi.org/10.1038/srep22377.

[19] S.O. Kasap, P. Capper, Springer Handbook of Electronic and Photonic Materials, Vol. 11, Springer, 2006.

[20] E. Arushanov, Crystal growth and characterization of II_3V_2 compounds, Progr. Cryst. Growth Charact. 3 (1980) 211–255, http://dx.doi.org/10.1016/0146-3535(80)90020-9.

[21] S. Khadhraoui, A. Triki, S. Hcini, S. Zemni, M. Oumezzine, Variable-range-hopping conduction and dielectric relaxation in $Pr_{0.6}Sr_{0.4}Mn_{0.6}Ti_{0.4}O_{3\pm\delta}$ perovskite, J. Magn. Magn. Mater. 371 (2014) 69–76, http://dx.doi.org/10.1016/j.jmmm.2014.07.044.

[22] H. Abdel-Khalek, M. Salam, A. El Mahalawy, The electrical conductivity and dielectric response of cupric acetylacetonate thin films, J. Electron. Mater. 48 (2019) http://dx.doi.org/10.1007/s11664-019-07138-1.

[23] T. Zangina, J. Hassan, K.A. Matori, R.S. Azis, U. Ahmadu, A. See, Sintering behavior, ac conductivity and dielectric relaxation of $Li_{1.3}Ti_{1.7}Al_{0.3}(PO_4)_3$ NASICON compound, Results Phys. 6 (2016) 719–725, http://dx.doi.org/10.1016/j.rinp.2016.10.003.

[24] S. Mazen, N. Abu-Elsaad, Structural, magnetic and electrical properties of the lithium ferrite obtained by ball milling and heat treatment, Appl. Nanosci. 5 (2014) 105–114, http://dx.doi.org/10.1007/s13204-014-0297-2.

[25] M. Stanguennec, S. Elliott, Frequency-dependent ionic conductivity in $AgI − AgPO_3$ glasses, Solid State Ion. 73 (1994) 199–208, http://dx.doi.org/10.1016/0167-2738(94)90035-3.

[26] A.F. Qasrawi, Effects of photoexcitation on the current transport mechanism in amorphous indium selenide thin films, Phil. Mag. 90 (2010) 3027–3035, http://dx.doi.org/10.1080/14786431003767041.

[27] V. Ambegaokar, B.I. Halperin, J.S. Langer, Hopping conductivity in disordered systems, Phys. Rev. B 4 (1971) 2612–2620, http://dx.doi.org/10.1103/PhysRevB.4.2612.

[28] V. Zakhvalinskii, E. Pilyuk, T. Nikulicheva, S. Ivanchikhin, M. Yaprintsev, T. Erina, Preparation and conduction mechanisms of thin films of dirac semimetal Cd_3As_2, Nauchnyye Vedomosti Belgorodskogo Gosudarstvennogo Univ. Seriya: Mat. Fizika 51 (2019) http://dx.doi.org/10.18413/2075-4639-2019-51-4-533-540.

[29] F. Mott N, A. Davis E, Electronic Processes in Non-Crystalline Materials, Clarendon Press, Oxford University Press, 1979.

[30] K. Morigaki, Physics of Amorphous Semiconductors, Imperial College Press, 1999.

[31] M. Chowdhury, P. Migliorato, J. Jang, Low temperature characteristics in amorphous indium-gallium-zinc-oxide thin-film transistors down to 10K, Appl. Phys. Lett. 103 (2013) http://dx.doi.org/10.1063/1.4824875.

[32] M.B. Bechir, K. Karoui, M. Tabellout, K. Guidara, A.B. Rhaiem, Alternative current conduction mechanisms of organic-inorganic compound $[N(CH_3)_3H]_2ZnCl_4$, J. Appl. Phys. 115 (2014) 153708, http://dx.doi.org/10.1063/1.4871662.

[33] S. Mahboob, G. Prasad, G. Kumar, Electrical conduction in $(Na_{0.125}Bi_{0.125}Ba_{0.65}Ca_{0.1})(Nd_{0.065}Ti_{0.87}Nb_{0.065})O_3$ ceramic, Bull. Mater. Sci. 29 (2006) 35, http://dx.doi.org/10.1007/BF02709353.

[34] A.A.A. Youssef, The permittivity and AC conductivity of the layered perovskite $[(CH_3)(C_6H_5)_3P]_2HgI_4$, Z. Naturforsch. A 57 (2002) 263–269, http://dx.doi.org/10.1515/zna-2002-0510.

[35] N. Ortega, A. Kumar, P. Bhattacharya, S.B. Majumder, R.S. Katiyar, Impedance spectroscopy of multiferroic $PbZr_xTi_{1-x}O_3/CoFe_2O_4$ layered thin films, Phys. Rev. B 77 (2008) 014111, http://dx.doi.org/10.1103/PhysRevB.77.014111.

[36] K. Funke, Jump relaxation in solid electrolytes, Progr. Solid State Chem. 22 (2) (1993) 111–195, http://dx.doi.org/10.1016/0079-6786(93)90002-9.

[37] K. Funke, P. Singh, R.D. Banhatti, Conductivity dispersion in supercooled calcium potassium nitrate: caged ionic motion viewed as part of standard behaviour, Phys. Chem. Chem. Phys. 9 (2007) 5582–5590, http://dx.doi.org/10.1039/B618788A.

[38] R. Kundu, D. Roy, S. Bhattacharya, Study of electrical transport of $Ag_2O − CdO − MoO_3$ glass-nanocomposite-semiconductor, ChemistrySelect 2 (2017) 6100–6108, http://dx.doi.org/10.1002/slct.201700255.

[39] R. Daou, N. Doiron-Leyraud, D. Le Boeuf, S. Li, F. Laliberté, O. Cyr-Choinière, Y. Jo, L. Balicas, J.-Q. Yan, J.-S. Zhou, J. Goodenough, L. Taillefer, Linear temperature dependence of resistivity and change in the Fermi surface at the pseudogap critical point of a high-Tc superconductor, Nat. Phys. 5 (2008) 31–34, http://dx.doi.org/10.1038/nphys1109.

[40] C. Collignon, S. Badoux, S.A. Ahmadi Afshar, B. Michon, F. Laliberté, O. Cyr-Choinière, J.-S. Zhou, S. Licciardello, S. Wiedmann, N. Doiron-Leyraud, L. Taillefer, Fermi-surface transformation across the pseudogap critical point of the cuprate superconductor $La_{1.6-x}Nd_{0.4}Sr_xCuO_4$, Phys. Rev. B 95 (2017) http://dx.doi.org/10.1103/PhysRevB.95.224517.

[41] C. Shekhar, A. Nayak, Y. Sun, M. Schmidt, M. Nicklas, I. Leermakers, U. Zeitler, W. Schnelle, J. Grin, C. Felser, B. Yan, Extremely large magnetoresistance and ultrahigh mobility in the topological weyl semimetal NbP, Nat. Phys. 11 (2015) 645–649, http://dx.doi.org/10.1038/nphys3372.

[42] F. Tafti, Q. Gibson, S. Kumar, N. Haldolaarachchige, R. Cava, Resistivity plateau and extreme magnetoresistance in $LaSb$, Nat. Phys. 12 (2015) 272–277, http://dx.doi.org/10.1038/nphys3581.

[43] S. Shanshan, Q. Wang, P.-J. Guo, K. Liu, H. Lei, Large magnetoresistance in $LaBi$: Origin of field-induced resistivity upturn and plateau in compensated semimetals, New J. Phys. 18 (2016) 082002, http://dx.doi.org/10.1088/1367-2630/18/8/082002.

[44] M. Ali, J. Xiong, S. Flynn, J. Tao, Q. Gibson, L. Schoop, T. Liang, N. Haldolaarachchige, M. Hirschberger, N. Ong, R. Cava, Large, non-saturating magnetoresistance in WTe_2, Nature 18 (2014) 205–208, http://dx.doi.org/10.1038/nature13763.

[45] K. Wang, D. Graf, L. Li, L. Wang, C. Petrovic, Anisotropic giant magnetoresistance in $NbSb_2$, Sci. Rep. 4 (2014) 7328, http://dx.doi.org/10.1038/srep07328.

[46] R. Singha, A.K. Pariari, B. Satpati, P. Mandal, Large nonsaturating magnetoresistance and signature of nondegenerate Dirac nodes in $ZrSiS$, Proc. Natl. Acad. Sci. 114 (10) (2017) 2468–2473, http://dx.doi.org/10.1073/pnas.1618004114.

[47] J. Hu, J. Liu, D. Graf, S. Radmanesh, D. Adams, A. Chuang, Y. Wang, I. Chiorescu, J. Wei, L. Spinu, Z. Mao, Berry phase and zeeman splitting of Weyl semimetal TaP, Sci. Rep. 6 (2016) 18674, http://dx.doi.org/10.1038/srep18674.

[48] J. Hu, T. Rosenbaum, Classical and quantum routes to linear magnetoresistance, Nature Mater. 7 (2008) 697–700, http://dx.doi.org/10.1038/nmat2259.

[49] M. Ali, Q. Gibson, S. Jeon, B. Zhou, A. Yazdani, R. Cava, The crystal and electronic structures of Cd_3As_2, the three-dimensional electronic analogue of graphene, Inorg. Chem. 53 (2014) 4062–4067, http://dx.doi.org/10.1021/ic403163d.

[50] C.-Z. Li, R. Zhu, X. Ke, J.-M. Zhang, L.-X. Wang, L. Zhang, Z.-M. Liao, D.-P. Yu, Synthesis and photovoltaic properties of Cd_3As_2 faceted nanoplates and nanooctahedrons, Cryst. Growth Des. 15 (7) (2015) 3264–3270, http://dx.doi.org/10.1021/acs.cgd.5b00399.

[51] H.T. Chorsi, S. Yue, P.P. Iyer, M. Goyal, T. Schumann, S. Stemmer, B. Liao, J.A. Schuller, Widely tunable optical and thermal properties of Dirac semimetal Cd_3As_2, Adv. Opt. Mater. 8 (8) (2020) 1901192, http://dx.doi.org/10.1002/adom.201901192.